Morphology, Crystallization, and Mechanical Properties of Poly(ethylene terephthalate)/Multiwalled Carbon Nanotubes Composites

Zhiguo Zhu,[1,2] Rui Wang,[1,2] Zhenfeng Dong,[1,2] Xiuqin Huang,[1,2] Dasheng Zhang[1,2]

[1]*Beijing Key Laboratory of Clothing Materials R&D and Assessment, Beijing 100029, People's Republic of China*
[2]*Department of Materials Science and Engineering, Beijing Institute of Clothing Technology, Beijing 100029, People's Republic of China*

Received 7 October 2008; accepted 12 September 2010
DOI 10.1002/app.33438
Published online 14 February 2011 in Wiley Online Library (wileyonlinelibrary.com).

ABSTRACT: Poly(ethylene terephthalate)/multiwalled carbon nanotubes (PET/MWCNTs) with different MWCNTs loadings have been prepared by *in situ* polymerization of ethylene glycol (EG) containing dispersed MWCNTs and terephthalic acid (TPA). From scanning electronic microscopy images of nanocomposites, it can be clearly seen that the PET/MWCNTs composites with low-MWCNTs contents (0.2 and 0.4 wt %) get better MWCNTs dispersion than analogous with high-tube loadings (0.6 and 0.8 wt %). The nonisothermal crystallization kinetics was analyzed by differential scanning calorimetry using Mo kinetics equation, and the results showed that the incorporation of MWCNTs accelerates the crystallization process obviously. Mechanical testing shows that, in comparison with neat PET, the Young's modulus and the yield strength of the PET nanocomposites with incorporating 0.4 wt % MWCNTs are effectively improved by about 25% and 15%, respectively. © 2011 Wiley Periodicals, Inc. J Appl Polym Sci 120: 3460–3468, 2011

Key words: carbon nanotubes; poly(ethylene terephthalate); nanocomposites; crystallization; mechanical properties

INTRODUCTION

Poly(ethylene terephthalate) (PET) is one of the most extensively applied thermoplastics, which is widely used in areas of packing, fiber, film, beverage bottles, and engineering plastics due to its high performance, good physical, and chemical properties as well as relatively low cost. As an engineering thermoplastic, however, PET shows some disadvantages that hinder its practical application in a more broad range of industry, including low rate of crystallization, low-thermal degradation temperature, and insufficient mechanical properties.[1]

Polymer nanocomposites are two-phase systems consisting of polymers loaded with high-surface-area reinforcing fillers. Such systems have attracted enormous interest from the materials community, because they theoretically promise substantial improvement on mechanical properties at very low-filler loadings.[2] In addition to motivating high level of interest for potential applications such as hydrogen storage, fuel cell, and field-emitting diode,[3–6] carbon nanotubes (CNTs) have been regarded as ideal nanofiller to polymer system in achieving high-performance polymer nanocomposites due to their extraordinary mechanical, electrical, and thermal properties.[7–9] Furthermore, the foreign CNTs can act as nucleating agents to promote crystallization rate of polymers including PET[10,11] and affect crystal sizes of PET and polypropylene[12] spherulites. The most generally accepted challenges in fabrication of polymer/CNTs composites with high performance might consist in the dispersion morphologies of CNTs in polymeric matrices and/or the interfacial interaction between CNTs and the matrices. Aiming to resolve above neck problem, melt blending,[13–17] solution blending,[18–21] and *in situ* polymerization,[22–26] as well as lateral technology,[27,28] solid-state shear, or mechanochemical pulverization,[29] are developed and extensively applied to prepare polymer nanocomposites containing pristine or functionalized[30] CNTs. In addition, coagulation spinning method was developed to produce composite fibers comprising predominately CNTs.[31]

As a part of research program on the fabrication and properties investigation of PET/CNTs nanocomposites, we report in this contribution the effects of the incorporation of multiwalled CNTs (MWCNTs) and the dispersion morphology of MWCNTs on the crystallization behavior and mechanical properties of PET/multiwalled CNTs (PET/MWCNTs) composites. PET

Correspondence to: Z. Zhu (zgzhu76@yahoo.cn).
Contract grant sponsor: Beijing Municipal Commission of Education; contract grant number: AJ2009-18.
Contract grant sponsor: Beijing Key Laboratory of Clothing Materials R & D and Assessment; contract grant number: 2007ZK-04.

nanocomposites with MWCNTs loadings ranging from 0.2 to 0.8 wt % were successfully fabricated by *in situ* polymerization of ethylene glycol (EG) containing dispersed MWCNTs and terephthalic acid (TPA). The resultant nanocomposites samples were characterized by means of scanning electronic microscope (SEM), differential scanning calorimetry (DSC), and Instron tensile tests of dog-bone-shaped specimens to clarify the effects of MWCNTs on the properties of PET/MWCNTs composites. Finally, the possible mechanism of mechanical reinforcement of CNTs is discussed. The results show that MWCNTs homogenously dispersed in PET facilitate obviously crystallization process of PET, resulting in the peak melt-crystallization temperature shifts to higher temperature. In addition, PET/MWCNTs composites show effective improvement in mechanical properties compared to neat PET.

EXPERIMENTAL

Materials

TPA and EG provided kindly by SinoPec Tianjin Co. were both industrial level products and used as received. All other reagents and solvents were purchased from Beijing Chemical Reagent Co. and used as received, unless otherwise mentioned. Multiwalled carbon nanotubes (MWCNTs, purity: 95–98%) obtained by thermal chemical vapor deposition method were purchased from Shenzhen Nanotech Port Co., China.[32] According to the supplier, the out-diameter and length are 10–20 nm and 5–15 μm, respectively. The as-received MWCNTs were dispersed in dilute nitric acid and stirred strongly for 48 h at room temperature to remove residual catalysts and other impurities. The purified MWCNTs, used in this study, were collected on a 0.2-μm-pore polytetrafluoroethylene membrane and washed with deionized water until neutrality.

Measurements

DSC (Seiko DSC 6200) analysis was performed under the nitrogen atmosphere. About 5 mg of polymer sample was heated to 295°C, staying for 7 min to eliminate the thermal history, and then cooled to 40°C. The heating and cooling rate were both 20°C/min. Nonisothermal crystallization kinetics was studied by cooling a sample from 295 to 50°C at different cooling rate, viz., 2.5, 5, 10, and 20°C/min. SEM (JSM-6360LV) was used to characterize the morphologies of MWCNTs and their dispersion states in PET matrix. Using a compression-molding machine, the dog-bone-shaped specimens with a dimension of 63.94 × 3.14 (width in middle part) × 0.92 mm^3 were molded at about 275°C under vacuum and then quenched to room temperature. The tensile test was carried out using an Instron universal material testing system (model 1122, with a load cell of 1.0 kN capacity) at 20°C with gauge length of 25 mm and crosshead speed of 5 mm/min. Property values given here represent an average of the results for at least five specimens.

Synthesis of PET and PET/MWCNTs nanocomposites

Typical procedure for poly(ethylene terephthalate)/multiwalled carbon nanotubes (PET/MWCNTs) with 0.2 wt % MWCNTs loading is given as below. (Note: the resulting nanocomposite was denoted as PET-2, and correspondingly, PET/MWCNTs composites containing 0.4, 0.6, and 0.8 wt % were named as PET-4, PET-6, and PET-8, respectively.)

Purified MWCNTs (0.25 g) were dispersed in EG (40.0 g and 0.64 mol) with the aid of ultrasonication at room temperature for 2 h. Approaching end of the dispersion, TPA (83.0 g and 0.5 mol) was charged with mechanical stirring. Into a 500-mL flask equipped with mechanical stirrer, distillation apparatus with condenser, and the suspension mixture of EG and TPA containing MWCNTs were added. The dark mixture was heated for about 3 h with the temperature kept between 245 and 255°C. Then, the resulting dark MWCNTs incorporated bis(2-hydroxyethyl) terephthalate was transferred into a home-made polycondensation reactor. The polycondensation was carried out at 280–290°C under reduced pressure (absolute pressure < 80 Pa) with Sb_2O_3 (33.2 mg) as catalyst. The reaction lasted for about 100 min. The final stirring power (or stirring electric current) was kept same to obtain similar molecular weight for each sample. With compression N_2 as protection atmosphere and impetus, PET nanocomposites melts were continuously extruded into cold water through the discharge die (5 mm in diameter) at the bottom of the reactor. The dark wire was collected and cut into chips. Neat PET was prepared with the same procedure as a control sample in measurements.

Intrinsic viscosity measurement

Relative viscosity (η_r) of solutions of PET and PET/MWCNTs series (c 0.1 g/dL) in the mixture of phenol and 1,1,2,2-tertachloroethane (1 : 1 by mass) were determined using an Ubbelohde viscometer (0.8 mm in capillary diameter) at constant temperature of 30°C ± 0.1°C. Before filtration through a grade-3 (G-3) sintered glass funnels into the viscometer, the solution was treated by centrifugation to remove suspended MWCNTs. The intrinsic viscosity ([η]) was calculated using a single-point determination method according to the following formulation (1).[33,34]

$$[\eta] = \frac{1}{c}\sqrt{2(\eta r - \ln \eta r - 1)} \quad (1)$$

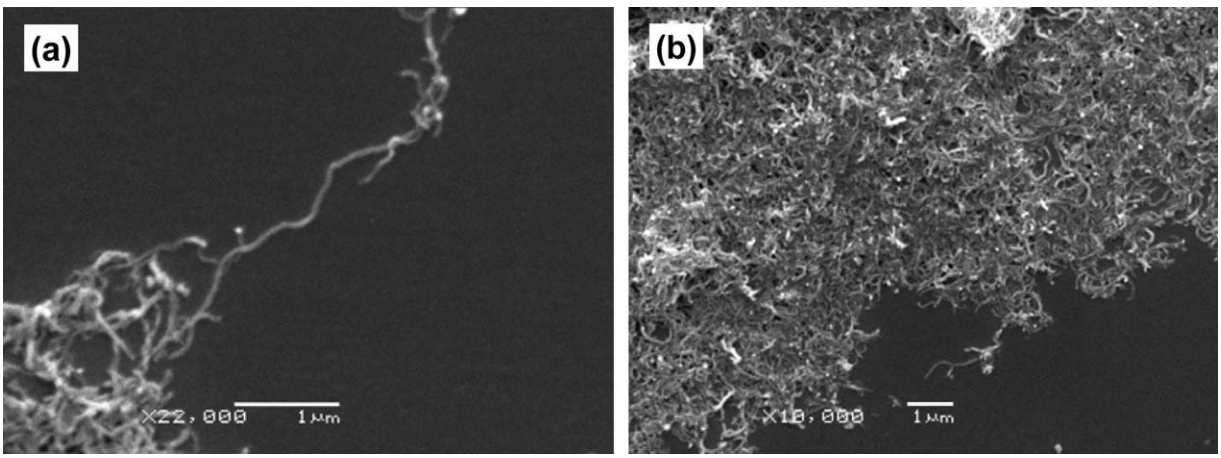

Figure 1 SEM images showing the morphology of MWCNTs before (a) and after acid purification (b).

RESULTS AND DISCUSSIONS

Morphology and dispersion of MWCNTs by SEM

Figure 1 shows the SEM images of the pristine and purified MWCNTs. It can be seen that both MWCNTs mainly exist in randomly aggregated entanglements due to strong intrinsic van der Waals attraction coupled with high-aspect ratio.[35] The MWCNTs were observed to be $\sim$ 30 nm in thickness and micron-scale in length. Purification in dilute nitric acid at room temperature had little influence on morphology of MWCNTs.

The esterification of EG and TPA in the presence of purified MWCNTs, followed by condensation

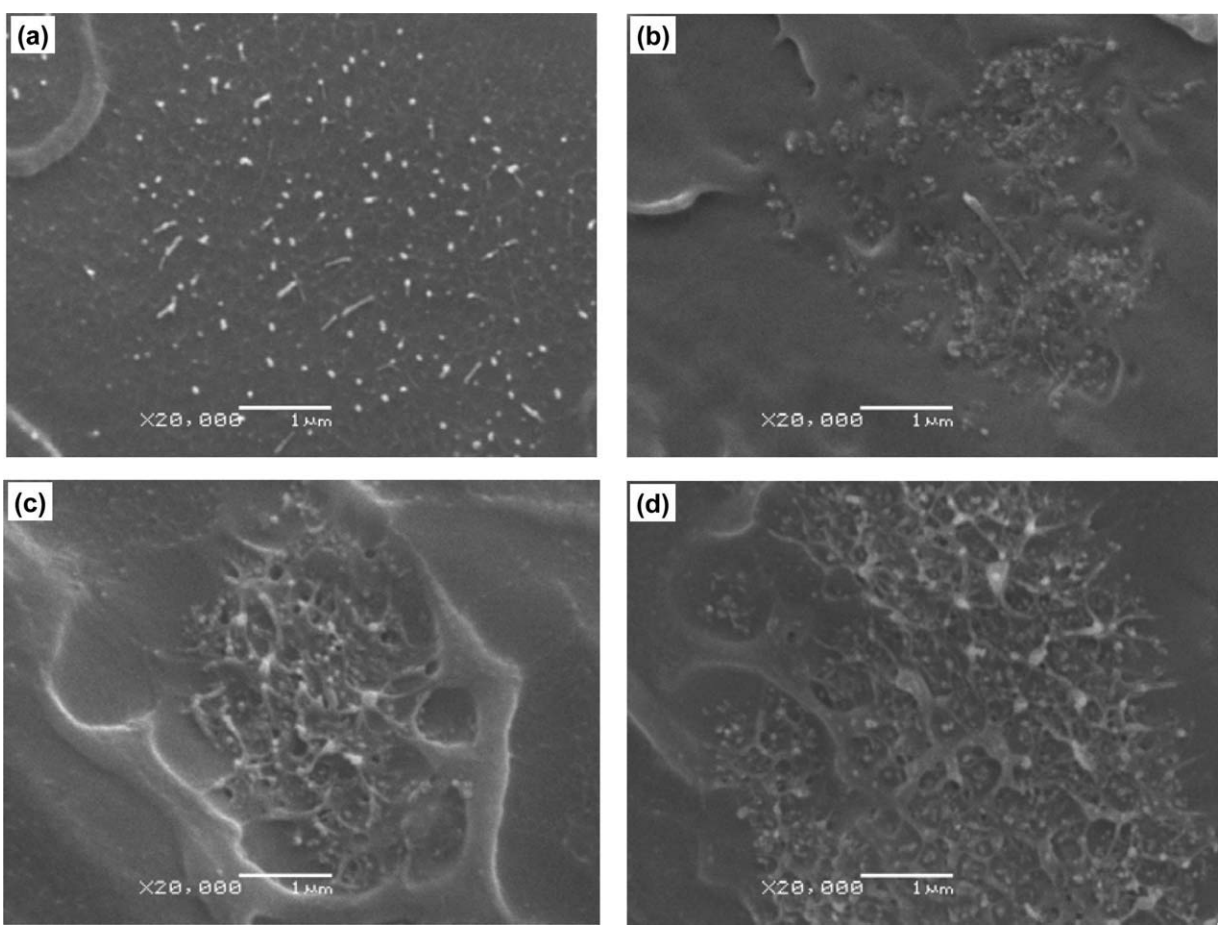

Figure 2 SEM images of cryogenically fractured surfaces of PET/MWCNTs nanocomposites: PET-2 (a), PET-4 (b), PET-6 (c), and PET-8 (d).

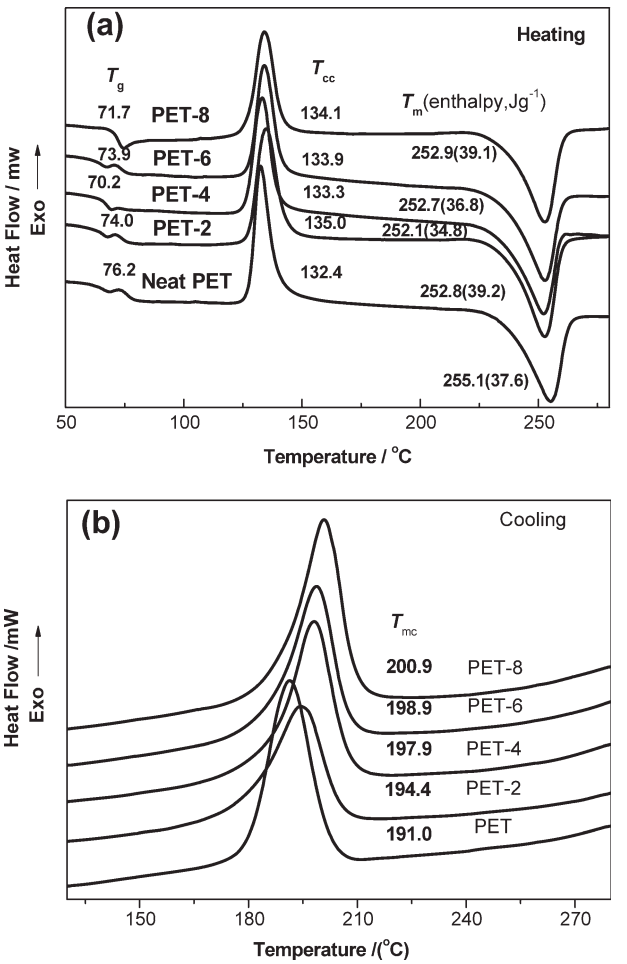

Figure 3 DSC curves of heating (a) and subsequent cooling (b) scans of quenched PET/MWCNTs samples with different MWCNTs loadings. The curves of neat PET were also given as comparison.

polymerization, was carried out to prepare *in situ* the respective PET/MWCNTs nanocomposites with different MWCNTs loadings. At the end of reaction, the molten polymer nanocomposites were extruded with nitrogen into cold water to form continuous polymer wires, which were macroscopically homogenous with uniform dark color.

Considering from typical concept on reinforcement mechanism of polymer containing reinforcement nanofillers,[36] however, the microdispersion morphology of CNTs plays a decisive role in achieving high performance for polymer composites as well as the strong interfacial interactions, so as to facilitate high-load transfer from the polymeric matrix to the fillers.[14,26]

Therefore, SEM was used to investigate the dispersion state of MWCNTs in polymer matrix. Cross sections of the nanocomposites were generated by breaking the composites wires frozen in liquid N_2, giving an intact surface fracture, and the SEM images are shown in Figure 2. The bright dots and lines are attributed to the MWCNTs, as mentioned in Refs. [15] and [26]. It can be seen from Figure 2(a) that the nanotubes dispersion is quite good. With increase of the loading of MWCNTs, a small number of agglomeration comprised few nanotubes was observed in PET-4 [Fig. 2(b)], while some dispersed MWCNTs were also noted. However, at higher MWCNTs contents, the aggregate size exceeds 1 μm [Fig. 2(c), PET-6], even reached a few microns [Fig. 2(d), PET-8]. Therefore, the formation of aggregates that initiated by concentration above 0.4 wt % might lead to a decrease of the surface area of the interface between MWCNTs and PET. This will give rise to variation in nucleation efficiency of MWCNTs on PET matrix, as discussed later.

Melting and crystallization characteristics

With the help of DSC, the melt and crystallization behaviors of PET nanocomposites were investigated. In the present work, quenched samples of PET and PET/MWCNTs composites were obtained during the extrusion into cold water through the discharge die. Because of the relatively low-crystallization rate, the amorphous state of PET is mainly obtained in the quenched samples, which is demonstrated by the obvious existence of glass-transition region, as shown in DSC curves. The DSC thermograms during heating run and subsequent cooling run are shown in Figure 3.

From the heating scan curves [Fig. 3(a)], it can be found that the glass transition temperature (T_g) tends to decrease with the addition of CNTs in PET, although there seems to show no obvious correlation between the tubes loadings and the values of T_g. For example, the T_g for PET-4 decreased by 6°C in comparison with neat PET (T_g, 76.2°C). On the other hand, Kim et al.[37] and Wu et al.,[38] respectively, found the increase in the T_g of poly(ethylene 2,6-naphthalate)/CNTs-COOH (PEN/*m*-CNT) and polylactide-*g*-acrylic acid/MWNTs-OH (PLA-*g*-AA/MWNTs-OH). The enhancement in T_g was both attributed to the hindrance of segmental motion of polymer macromolecular chains through strong interfacial bonds between the polar group from modified CNTs and polymers. According to Yuen's results on polyimide/CNTs (PI/CNTs) composites,[39] the T_g of the polymer matrix depended on the free volume of the polymer, which is related to the affinity between the CNTs and the polymer matrix. Compared to modified CNTs, unmodified MWCNTs used in our present work have a poor affinity (or surface wetting[40]) toward PET matrix, increasing the free volume beyond that of neat PET, thus leading a slight decrease in T_g with incorporation of CNTs in PET matrix.

Furthermore, as shown in Figure 3(a), the nucleation effect of MWCNTs in cold-crystallization

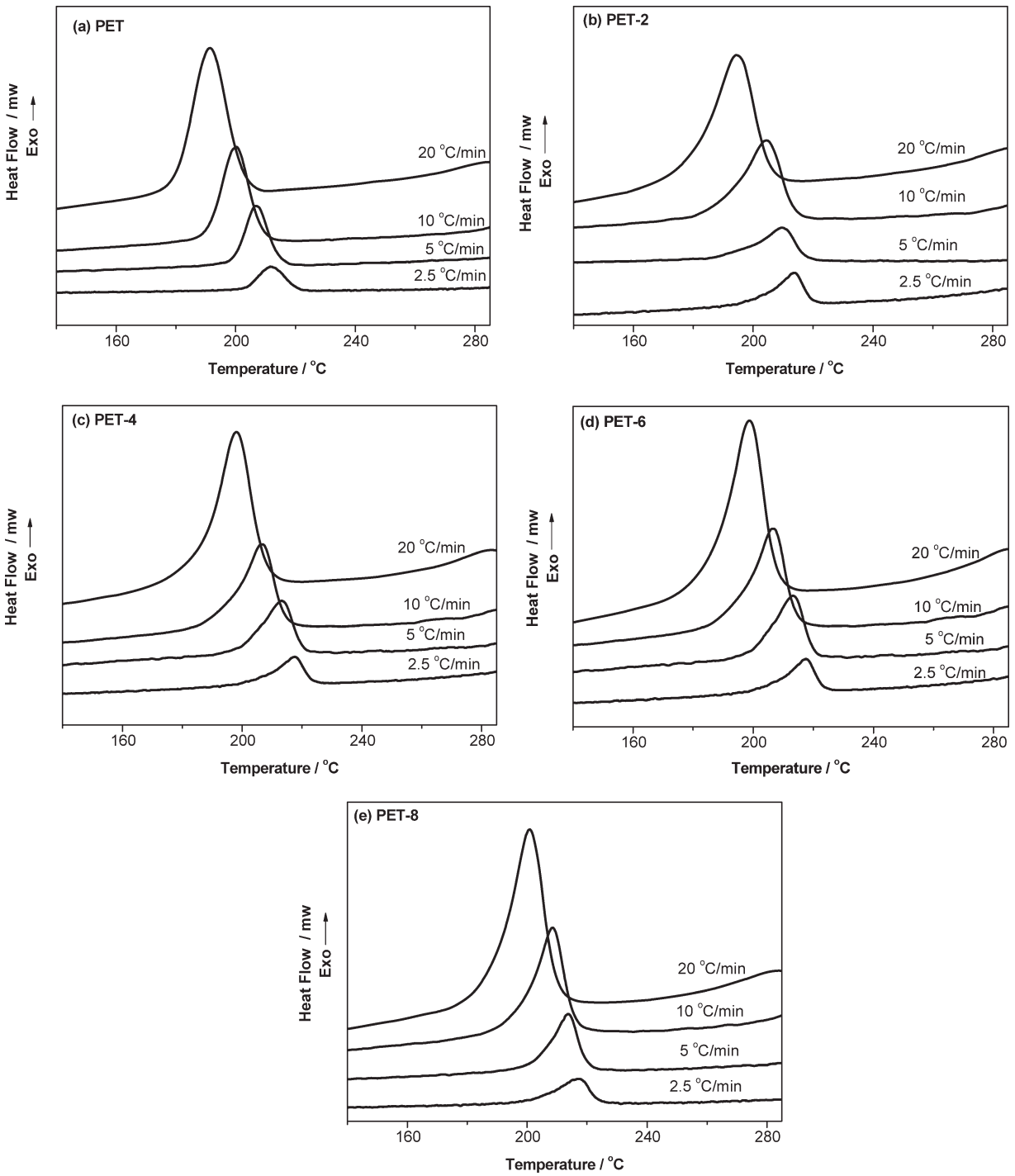

Figure 4 DSC cooling curves of PET (a), PET-2 (b), PET-4 (c), PET-6 (d), and PET-8 (e) at different cooling rates.

behavior[41,42] was not apparent, even with the peak cold-crystallization temperature (T_{cc}) shifting to higher temperatures after incorporating MWCNTs in PET. It might be attributed to the complexity of cold-crystallization process due to the pre-existence of crystal domains. The melting temperature (T_m) and enthalpies of PET stay almost unaffected by MWCNTs. Similar results were also obtained by Agarwal and coworkers addressing the effect of CNTs on the rate of PET crystallization.[10]

However, MWCNTs obviously acted as nucleation agent in crystallization from melt. Figure 3(b) shows the DSC cooling scans of neat PET and PET/MWCNTs composites samples.

During cooling run from melt with thermal history erased by 7 min staying at 295°C, the nanocomposites show crystallization exotherms much earlier than neat PET. With increasing the MWCNTs contents from 0.2 to 0.8 wt % in PET, the melt-crystallization behavior was influenced with the peak temperature

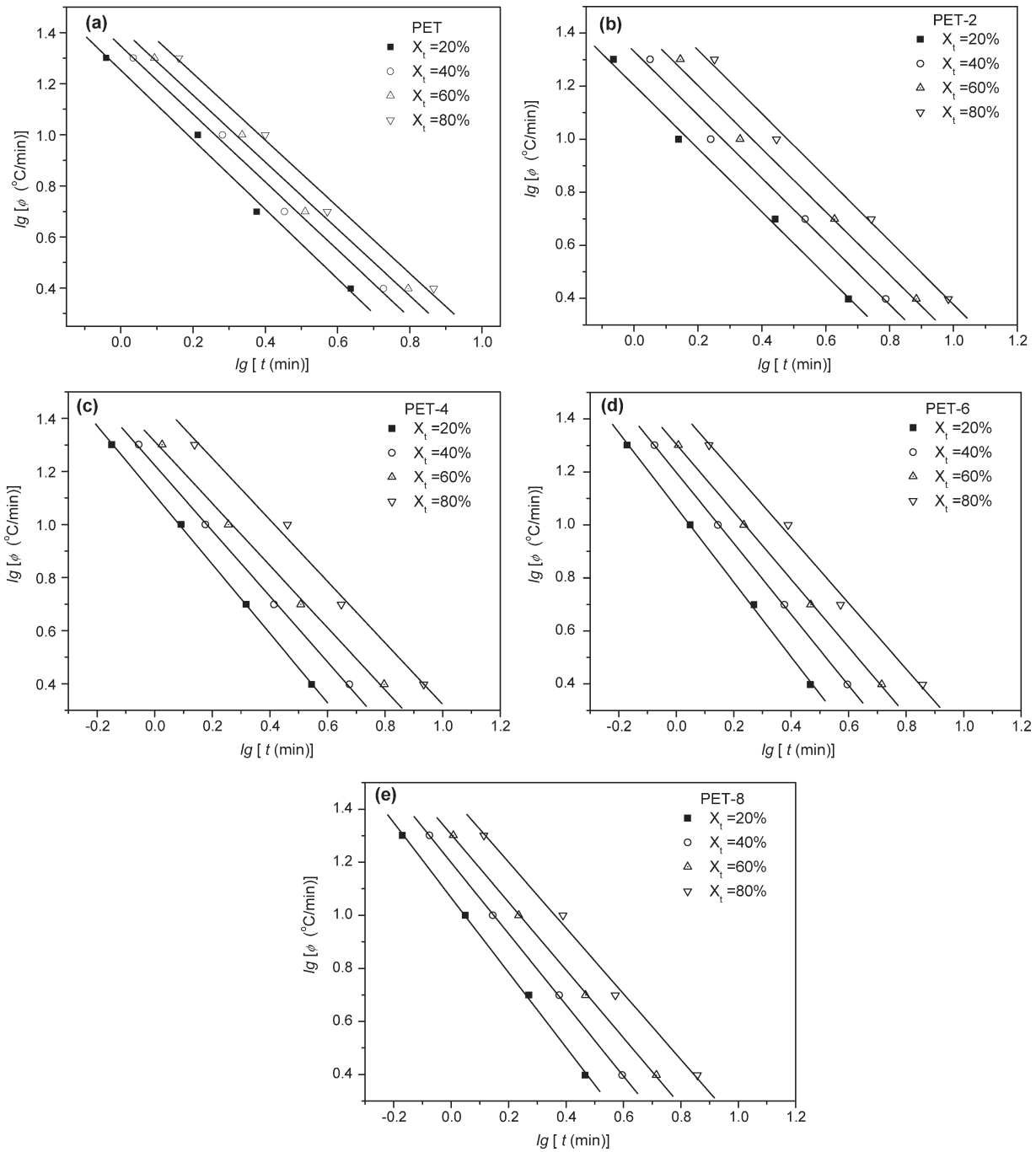

Figure 5 Plots of log ϕ versus log t based on Mo model at different relative degree of crystallinity (X_t) for PET (a), PET-2 (b), PET-4 (c), PET-6 (d), and PET-8 (e).

(T_{mc}) increasing up to 201°C, about 10°C higher than that of neat PET. This suggests that the crystallization ability of polymers melt was enhanced, obviously due to the nucleation effect of the foreign CNTs. Note that it shows little change in T_{mc} when the loading of CNTs was increased from 0.4 wt % to 0.6 wt %. This might be due to the heterogeneous dispersion of MWCNTs in PET-6, demonstrating by formation of large scale CNTs aggregates in SEM image [Fig. 2(c)].

As heterogeneous nucleating agent, the nucleation efficiency of MWCNTs is greatly determined by the distribution of nucleating sites in polymer matrix,[43] or in other words, by the interfacial area between nucleating agent and polymer chain. The formation of aggregation that initiated by concentration of MWCNTs led to decrease of the contact area between the MWCNTs and PET, thus give rise to decrease in nucleating efficiency. On the other hand, the disadvantageous effect from aggregation is somewhat balanced by the amount increment of CNTs, exhibiting almost no change in T_{mc} between PET-4 and PET-6. Furthermore, PET-8 shows peak

TABLE I
Nonisothermal Crystallization Kinetics Parameters of PET and PET Nanocomposites

Sample	$X(t)$ (%)	log [$F(T)$]	α
PET	20	1.25	1.36
	40	1.35	1.33
	60	1.42	1.31
	80	1.50	1.30
PET-2	20	1.20	1.19
	40	1.33	1.19
	60	1.44	1.19
	80	1.58	1.20
PET-4	20	1.11	1.30
	40	1.22	1.24
	60	1.31	1.17
	80	1.48	1.15
PET-6	20	1.07	1.41
	40	1.20	1.34
	60	1.30	1.28
	80	1.45	1.24
PET-8	20	1.10	1.40
	40	1.22	1.33
	60	1.32	1.27
	80	1.44	1.23

melt-crystallization temperature at higher temperature than PET-4 and PET-6 do, although more severe aggregation occurred [Fig. 3(d)]. All these results indicated that crystal formation of PET/MWCNTs systems was thermodynamically more favorable than that of neat PET at higher temperature, originating from the nucleation effect of CNTs in PET matrix.

Nonisothermal crystallization kinetics

Nonisothermal crystallization of neat PET and nanocomposites samples is studied at four different cooling rates, viz., 2.5, 5, 10, and 20°C/min. The DSC cooling curves are shown as Figure 4.

Combining the Avrami equation[44,45] on isothermal crystallization kinetics and Ozawa equation[46] on nonisothermal conditions, Mo et al.[47] developed a novel kinetic equation of nonisothermal crystallization as below.

$$\lg Z_t + n \lg t = \lg K(T) - m \lg \phi \tag{2}$$

and further rewritten as

$$\lg \phi = \lg F(T) - \alpha \lg t \tag{3}$$

where Z is a composite crystallization rate constant involving both nucleation and growth rate, $K(T)$ is cooling or heating function, and the kinetic parameter $F(T) = [K(T)/Z_t]^{1/m}$ refers to the value of cooling rate ϕ, which has to be chosen at unit crystallization time when the measured system amounts to a defined relatively degree of crystallinity (X_t). α is the ratio of Avrami exponent n to the Ozawa exponent m, the value of which depends on the type of nucleation and the dimensions of the crystal growth. Therefore, at a given X_t, the plots of log ϕ versus log t will give a straight line with the intercept of log $F(T)$ and the slope of α, just shown as Figure 5 and Table I.

The result show that, at certain crystallization time, a higher cooling rate resulted in a higher X_t. In addition, one can see from Figure 5 that the time used to obtain the same relative degree of crystallinity fell into a decrease tendency with increasing the MWCNTs contents in PET matrix, when the cooling rate was kept unchanged. It indicated that the MWCNTs accelerate the crystallization of PET chain probably attributed to its nucleation effects. The variation of α indicated that the addition of MWCNTs influenced the nonisothermal crystallization process via acting on type of nucleation and dimensions of crystal growth.

Tensile property and fracture morphology

Mechanical properties representing an average of the results from at least five specimens are reported as Table II. It can be seen that addition of MWCNTs effectively improves the tensile properties of PET matrix. Upon incorporation of 0.4 wt % MWCNTs, the elastic modulus (Young's modulus) of PET is improved by about 25% from 1.78 to 2.22 GPa, and the tensile strength at yield is improved by about 15% from 42.22 to 49.26 MPa. The elongation at break greatly decreases by addition lower MWCNTs weight fraction, that is, 0.2 and 0.4 wt %, indicating that the composites become much brittle. However, with the addition of 0.6 and 0.8 wt % MWCNTs, PET nanocomposites again exhibit large elongation at break, viz., 141 and 135%, respectively. It is probably due to the poor dispersion of MWCNTs in these two composites [see Fig. 2(c,d)]. The micron-scale aggregates decreased the reinforcement efficiency of MWCNTs because of decrease of the interface area. Correspondingly, the strength at yield and Young's modulus for

TABLE II
Summary of Mechanical Properties of Neat PET and Its Nanocomposites

Samples	[η][a] (dL g^{-1})	Tensile strength[b] (MPa)	Elongation at break (%)	Young's modulus (GPa)
Neat PET	0.637	42.22 ± 5.42	125 ± 21	1.78 ± 0.16
PET-2	0.697	48.87 ± 1.19	37 ± 7	1.99 ± 0.06
PET-4	0.679	49.26 ± 1.08	33 ± 6	2.22 ± 0.07
PET-6	0.721	47.39 ± 0.77	141 ± 25	2.01 ± 0.03
PET-8	0.685	47.86 ± 0.40	135 ± 8	2.08 ± 0.04

[a]The intrinsic viscosity calculated according to single point determination relationship.
[b]Strength at yield.

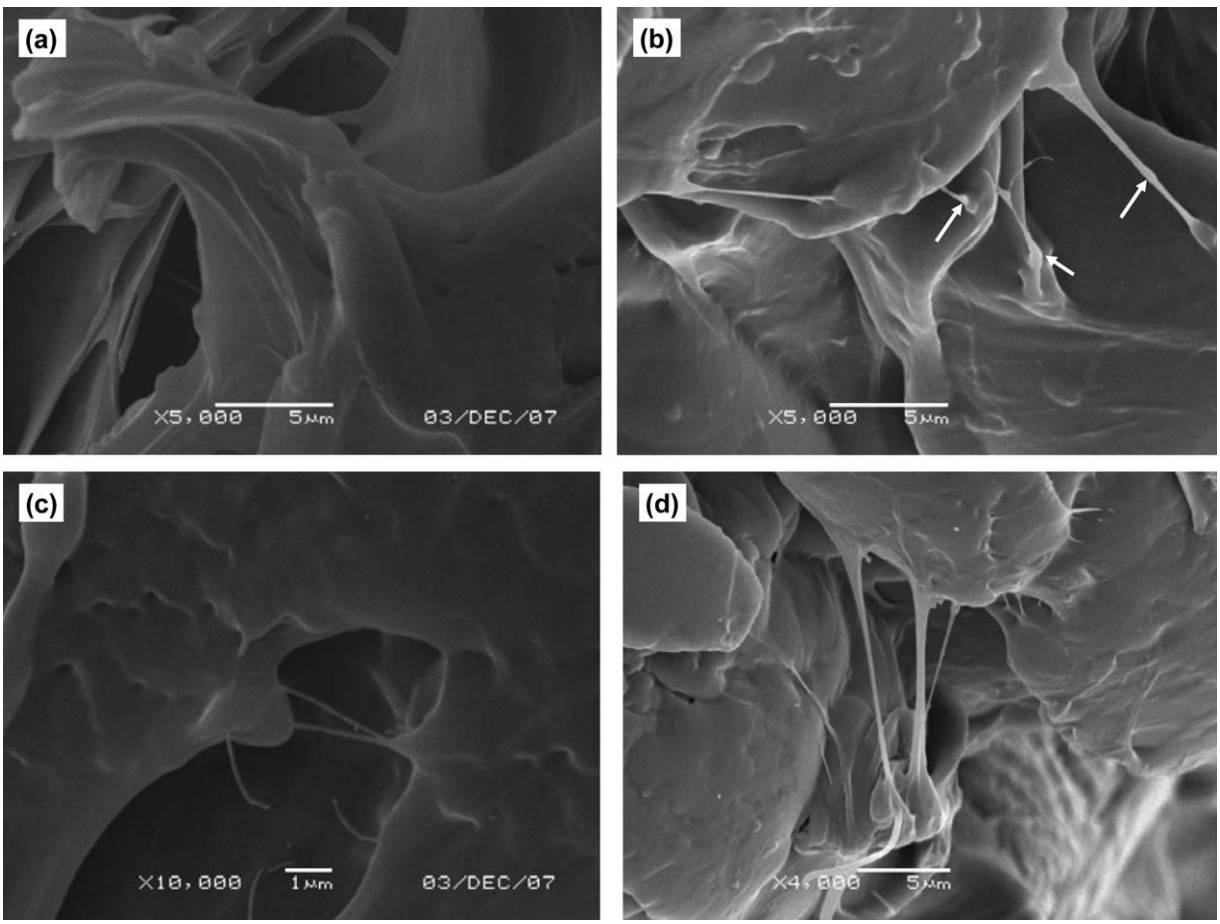

Figure 6 SEM images showing the morphology of failure fracture for neat PET (a), PET-2 (b,c), and PET-4 (d).

samples PET-6 and PET-8 began to decrease in comparison with those of PET-4.

From the SEM image of the failure fracture after tensile test, some possible reinforcing mechanism could be drawn. Figure 6 shows the fracture surfaces of the samples PET-2 and PET-4, with the image of neat PET given for comparison. Upon tensile failure, some beltlike structures were observed, which connect two polymer lumps, and the middle part of the stretched architectures is thinner than the two ends adhered to the polymer matrix. Moreover, some nanotubes were found to be broken, with the ends embedded into the polymer lumps [Fig. 6(c)]. Obviously, the interconnection fiberlike structures consist of individual tube or tube bundle coated by polymer, because their diameters are much lager than MWCNTs' diameter shown in Figure 1. Interestingly, several small bump or beadlike morphology was observed along the stretched fiberlike structure, as shown by arrow in Figure 6(b). Compared to that of neat PET, the interesting and distinct breakage morphology for PET nanocomposites indicated the existence of interfacial affinity between MWCNTs and PET matrix. These should be contributed to the increase of strength and modulus for PET after incorporation of MWCNTs, as listed in Table II.

Detailed studies needed to be conducted to achieve high-reinforcement efficiency and to fully understand the mechanical reinforcement role of CNTs in PET matrix, including (1) incorporation organic functionalized CNTs to improve the dispersion state and interfacial adhesion interaction, especially for high-tube loadings and (2) enhancing the alignment of tubes in polymer matrix by drawing into nanocomposite fibers.[48] Furthermore, other properties coupled with PET nanocomposites containing CNTs, such as electrical conductivity and flame retardancy,[49] are also in progress.

CONCLUSIONS

In situ polycondensation between the EG and TPA in the presence of dispersed MWCNTs with weight fraction ranged from 0.2 to 0.8 wt % had resulted in moderate intrinsic viscosity PET as the matrix of the nanocomposites. With low-MWCNTs loadings, homogenous dispersion morphology of MWCNTs in PET was demonstrated by SEM observation, while obvious aggregates formed when MWCNTs loading exceeds 0.4 wt %. DSC nonisothermal crystallization kinetics analysis indicated that MWCNTs acted as

heterogeneous nuclei in melt-crystallization process. Mechanical test shows that, in comparison with neat PET, the tensile strength and Young's modulus are effectively improved by about 15 and 25%, respectively, with incorporating 0.4 wt % MWCNTs. SEM results indicate that the homogenous dispersion of MWCNTs and interfacial adhesion between MWCNTs and PET was believed to be responsible for the enhancement in mechanical properties.

References

1. Scheirs, J.; Long, T., Eds. Modern Polyesters: Chemistry and Technology of Polyesters and Copolyesters. Wiley: Hoboken, NJ, 2003.
2. Schaefer, D. W.; Justice, R. S. Macromolecules 2007, 40, 8501.
3. Baughman, R. H.; Zakhidov, A. A.; de Heer, W. A. Science 2002, 297, 787.
4. Liu, C.; Fan, Y. Y.; Liu, M.; Cong, H. T.; Cheng, H. M.; Dresselhaus, M. S. Science 1999, 286, 1127.
5. Han, S. J.; Yun, Y. K.; Park, K. W.; Sung, Y. E.; Hyeon, T. Adv Mater 2003, 15, 1922.
6. Dalton, A. B.; Collins, S.; Munoz, E.; Razal, J. M.; Ebron, V. H.; Ferraris, J. P.; Coleman, J. N.; Kim, B. G.; Baughman, R. H. Nature 2003, 423, 703.
7. Iijima, S. Nature 1991, 354, 56.
8. Ajayan, P. M. Chem Rev 1999, 99, 1787.
9. Moniruzzaman, M.; Winey, K. I. Macromolecules 2006, 39, 5194.
10. Anand, A. K.; Agarwal, U. S.; Joseph, R. Polymer 2006, 47, 3976.
11. Anand, A. K.; Agarwal, U. S.; Nisal, A.; Joseph, R. Eur Polym J 2007, 43, 2279.
12. Valentini, L.; Biagiotti, J.; Lopez-Manchado, M. A.; Santucci, S.; Kenny, J. M. Polym Eng Sci 2004, 44, 303.
13. Poetschke, P.; Bhattacharyya, A. R.; Janke, A.; Goering, H. Compos Interfaces 2003, 10, 389.
14. Liu, T. X.; Phang, I. Y.; Shen, L.; Chow, S. Y.; Zhang, W. D. Macromolecules 2004, 37, 7214.
15. Zhang, W. D.; Shen, L.; Phang, I. Y.; Liu, T. X. Macromolecules 2004, 37, 256.
16. Bhattacharyya, A. R.; Sreekumar, T. V.; Liu, T.; Kumar, S.; Ericson, L. M.; Hauge, R. H.; Smalley, R. E. Polymer 2003, 44, 2373.
17. Siochi, E. J.; Working, D. C.; Park, C.; Lillehei, P. T.; Rouse, J. H.; Topping, C. C.; Bhattacharyya, A. R.; Kumar, S. Compos B 2004, 35, 439.
18. Haggenmueller, R.; Fischer, J. E.; Winey, K. I. Macromolecules 2006, 39, 2964.
19. Islam, M. F.; Rojas, E.; Bergey, D. M.; Johnson, A. T.; Yodh, A. G. Nano Lett 2003, 3, 269.
20. Koganemaru, A.; Bin, Y.; Agari, Y.; Matsuo, M. Adv Funct Mater 2004, 14, 842.
21. Sabba, Y.; Thomas, E. L. Macromolecules 2004, 37, 4815.
22. Bryning, M. B.; Milkie, D. E.; Islam, M. F.; Kikkawa, J. M.; Yodh, A. G. Appl Phys Lett 2005, 87, 161909/1.
23. Zhu, J.; Kim, J.; Peng, H.; Margrave, J. L.; Khabashesku, V. N.; Barrera, E. V. Nano Lett 2003, 3, 1107.
24. Gong, X.; Liu, J.; Baskaran, S.; Voise, R. D.; Young, J. S. Chem Mater 2000, 12, 1049.
25. Moniruzzaman, M.; Du, F.; Romero, N.; Winey, K. I. Polymer 2006, 47, 293.
26. Gao, J.; Zhao, B.; Itkis, M. E.; Bekyarova, E.; Hu, H.; Kranak, V.; Yu, A.; Haddon, R. C. J Am Chem Soc 2006, 128, 7492.
27. Regev, O.; ElKati, P. N. B.; Loos, J.; Koning, C. E. Adv Mater 2004, 16, 248.
28. Dufresne, A.; Paillet, M.; Putaux, J. L.; Canet, R.; Carmona, F.; Delhaes, P.; Cui, S. J Mater Sci 2002, 37, 3915.
29. Xia, H,; Wang, Q.; Li, K.; Hu, G. H. J Appl Polym Sci 2004, 93, 378.
30. Sun, Y. P.; Fu, K.; Huang, W. J. Acc Chem Res 2002, 35, 1096.
31. Vigolo, B.; Penicaud, A.; Coulon, C.; Sauder, C.; Pailler, R.; Journet, C.; Bernier, P.; Poulin, P. Science 2000, 290, 1331.
32. http://www.seasunnano.com.
33. Liu, Y. J. Macromol Mater Eng 2001, 286, 611.
34. Ma, Y.; Agarwal, U. S.; Sikkema, D. J.; Lemstra, P. J. Polymer 2003, 44, 4085.
35. Calvert, P. Nature 1999, 399, 210–211.
36. Coleman, J. N.; Khan, U.; Blau, W. J.; Gun'ko, Y. K. Carbon 2006, 44, 1624.
37. Kim, J. Y.; Han, S.; Hong, S. Polymer 2008, 49, 3335.
38. Wu, C. S.; Liao, H. T. Polymer 2007, 48, 4449.
39. Yuen, S. M.; Ma, C. C. M.; Lin, Y. Y.; Kuan, H. C. Compos Sci Technol 2007, 67, 2564.
40. Rittigstein, P.; Torkelson, J. M. J Polym Sci Part B: Polym Phys 2006, 44, 2935.
41. Lee, H. J.; Oh, S. J.; Choi, J. Y.; Kim, J. W.; Han, J.; Tan, L. S.; Baek, J. B. Chem Mater 2005, 17, 5057.
42. Gao, Y.; Wang, Y.; Shi, J.; Bai, H.; Song, B. Polym Test 2008, 27, 179.
43. Hu, G.; Feng, X.; Zhang, S.; Yang, M. J Appl Polym Sci 2008, 108, 4080.
44. Avrami, M. J Chem Phys 1939, 7, 1103.
45. Avrami, M. J Chem Phys 1940, 8, 212.
46. Ozawa, T. Polymer 1971, 12, 150–158.
47. Liu, T. X.; Mo, Z. S.; Wang, S. E.; Zhang, H. F. Polym Eng Sci 1997, 37, 568–575.
48. Potschke, P.; Brunig, H.; Janke, A.; Fischer, D.; Jehnichen, D. Polymer 2005, 46, 10355–10363.
49. Kashiwagi, T.; Du, F.; Douglas, J. F.; Winey, K. I.; Harris, R. H.; Shields, J. R. Nat Mater 2005, 4, 928–933.